

Disentangling Atmospheric Compositions of K2-18 b with Next Generation Facilities

Q. CHANGEAT,¹ B. EDWARDS,¹ A. F. AL-REFAIE,¹ A. TSIARAS,¹ I.P. WALDMANN,¹ AND G. TINETTI¹

¹*Department of Physics and Astronomy
 University College London
 Gower Street, WC1E 6BT London, United Kingdom*

Submitted to AJ

ABSTRACT

Recent analysis of the planet K2-18 b has shown the presence of water vapour in its atmosphere. While the H₂O detection is significant, the Hubble Space Telescope (HST) WFC3 spectrum suggests three possible solutions of very different nature which can equally match the data. These solutions include a primary cloudy atmosphere with traces of water vapour and a secondary atmosphere with a substantial amount of H₂O and/or an undetectable gas such as N₂. Additionally, the atmospheric pressure and the possible presence of a liquid/solid surface cannot be investigated with currently available observations.

In this paper we used the best fit parameters from Tsiaras et al. (2019) to build JWST and Ariel simulations of the three scenarios. We have investigated 18 retrieval cases, which encompass the three scenarios and different observational strategies with the two observatories.

Retrieval results show that twenty combined transits should be enough for the Ariel mission to disentangle the three scenarios, while JWST would require only two transits if combining NIRISS and NIRSpec data. This makes K2-18 b an ideal target for atmospheric follow-ups by both facilities and highlights the capabilities of the next generation of space-based infrared observatories to provide a complete picture of low gravity planets.

1. INTRODUCTION

Recent observations of K2-18 b with the Hubble Space Telescope (HST) have, for the first time, revealed the presence of water vapour in the atmosphere of a low gravity planet orbiting within the habitable-zone of its star. This detection, published by two independent studies, Tsiaras et al. (2019) and Benneke et al. (2019), is particularly exciting if compared with the featureless atmospheric signals observed so far in the Super-Earth/Sub-Neptune regime. However, while the water vapour feature is evident in the HST-WFC3 observations, it is not possible to constrain its abundance, in particular relative to H/He and other undetectable gases. The narrow wavelength coverage of the HST-WFC3 camera does not allow to disentangle among a primary atmosphere, i.e. mainly composed of H/He, or a secondary atmosphere, i.e. an atmosphere which has evolved from the primordial composition and contains

a non negligible fraction of gases other than H/He. To capture the variety of possible cases which could explain current WFC3 observations, three main scenarios were identified in Tsiaras et al. (2019): these are summarised here:

1. A secondary atmosphere with a mean molecular weight explained by water vapour (up to 50%) additionally to H/He.
2. A secondary atmosphere with traces of water vapour additionally to one or multiple undetectable absorbers (e.g. N₂) and H/He.
3. A cloudy primary atmosphere composed mainly by H/He and traces of water vapour.

Most importantly, the thickness of the atmosphere cannot be inferred from the HST-WFC3 observations. This information is critical to constrain the bulk nature of the planet, i.e. whether K2-18 b is an Ocean planet with a liquid surface or there is a thick H/He atmosphere.

In this paper, we simulate the ability of the James Webb Space Telescope (JWST) and the European

Corresponding author: Q. Changeat
 quentin.changeat.18@ucl.ac.uk

Opacity	References
H ₂ -H ₂	Abel et al. (2011), Fletcher et al. (2018)
H ₂ -He	Abel et al. (2012)
H ₂ O	Barton et al. (2017), Polyansky et al. (2018)

Table 1. List of opacities used in this work

Space Agency Ariel mission to observe K2-18 b’s atmosphere. We then use spectral retrieval models to interpret the simulated observations. Finally, we discuss future prospects to understand the nature of this interesting planet in light of our simulations.

2. METHODOLOGY

2.1. Overview

To simulate various chemical compositions and structures of the atmosphere of K2-18 b and conclude on their detectability, we performed both forward radiative transfer models and inverse models (spectral retrievals) using the open-source Bayesian framework TauREx3 (Al-Refaie et al. (2019), which is a more efficient and comprehensive version of TauRex (Waldmann et al. (2015a), Waldmann et al. (2015b)). TauREx is a fully Bayesian radiative transfer code which include the highly accurate molecular line-lists from the ExoMol project (Tennyson et al. (2016)), HITEMP (Rothman & Gordon (2014)) and HITRAN (Gordon et al. (2016)). The complete list of opacities used in this paper can be found in Table 1. TauREx3 is available on GitHub ¹ and is optimised for Windows, Mac and Linux.

We followed a three-step approach. We started by simulating the three scenarios described in Tsiaras et al. (2019), i.e. a secondary atmosphere with comparable amount of H/He and water vapour, a secondary atmosphere with comparable amount of H/He and N₂ and traces of water vapour, a primary H/He atmosphere with clouds and traces of water vapour. The parameters used in these forward models are detailed in Table 2.

Transit spectra were generated with TauREx3 at high resolution and then binned to the resolution of the observations. To simulate JWST and Ariel performances, we used the noise simulators ExoWebb (Edwards et al. 2019a) for JWST and ArielRad (Mugnai et al. 2019) for Ariel. We assumed the JWST observations are performed with NIRISS and NIRSpec, therefore the total number of observations reported here should be interpreted as equally split between these two instruments. The combination of NIRISS and NIRSpec ensure an op-

Parameter	Model 1	Model 2	Model 3
radius (R _J)	0.219	0.219	0.216
temperature (K)	286	286	288
H ₂ O/H ₂	0.541	3.71 × 10 ⁻⁴	1.28 × 10 ⁻³
N ₂ /H ₂	7.82 × 10 ⁻⁷	0.0592	6.74 × 10 ⁻⁷
P _{clouds} (bar)	2.85	2.85	6.92 × 10 ⁻²

Table 2. Parameters adopted to describe the three atmospheric scenarios described in Tsiaras et al. (2019). Model 1: secondary atmosphere with comparable amount of H/He and H₂O. Model 2: secondary atmosphere with comparable amount of H/He and N₂ and traces of H₂O. Model 3: primary H/He atmosphere with clouds and traces of H₂O.

Parameter	NIRISS	NIRSpec
Filter/Grism	GR700XD ORD1	F290LP-G395m
Spectral Coverage [μm]	0.83 - 2.81	2.87 - 5.27
Number Groups	31	25
Timer [s]	164.7	21.7
Max Saturation Level	78%	78%
In Transit Integrations	58	430
Out Transit Integrations	116	860

Table 3. JWST instrument setups used in ExoWebb for this work which utilises the latest version of Pandeia Pontoppidan et al. (2016).

timal wavelength coverage from 0.8 μm to 5 μm: the instrument setup chosen is summarised in Table 3. When performing the retrievals, we do not scatter simulated observed spectra for the reasons outlined in Feng et al. (2018) and Changeat et al. (2019).

The simulated observed spectra were then used as input to TauREx3, retrieval mode, to analyse their information content and assess, by inspection of the posteriors, whether the three atmospheric scenarios could be disentangled.

2.2. Forward model assumptions

As the nature of K2-18 b is still poorly known, we have adopted very basic assumptions in our forward models. As in Tsiaras et al. (2019), we have assumed isothermal and isocompositional atmospheres; clouds are simulated using a basic grey cloud model, where the atmosphere is completely opaque below a given pressure. We included absorptions from H₂O and N₂, Collision Induced Absorption (CIA) opacities for H₂-H₂ and H₂-He and Rayleigh scattering (Cox 2015). N₂, being an inactive species, contributes only to the continuum and does not show molecular features. We expressed abundances as ratios of H/He. This allows an easier comparison of our retrieval results and ensures an optimal sampling of the parameter space (i.e. no boundary effect around mixing ratios of 1).

¹ http://github.com/ucl-exoplanets/Taurex3_public

Telescope	number transit	resolution
JWST	2	30
JWST	10	100
JWST	20	100
Ariel	10	10/12/10
Ariel	20	10/12/10
Ariel	50	10/50/15

Table 4. Simulations of K2-18 b with JWST and Ariel as reported in this paper. The number of transits considered and the spectral resolutions are indicated.

Parameter	mode	prior
radius (R_J)	linear	$0.01 - 0.5$
temperature (K)	linear	$50 - 600$
H_2O/H_2	log	$10^{-5} - 10$
N_2/H_2	log	$10^{-5} - 10$
P_{clouds} (bar)	log	$10^1 - 10^{-5}$

Table 5. Free parameters and uniform priors adopted in the retrievals

For both missions we investigated three cases by varying the number of observed transits. The list of investigated cases is summarised in Table 4. Being K2-18 a relatively faint star and K2-18 b a small and cold planet, this target is challenging for Ariel, so a larger number of stacked transits is considered compared to JWST. As this planet has an orbital period of approximately thirty-two days, we restrain the maximum number of observed transits to fifty.

2.3. Retrieval Model Assumptions

We performed, in total, eighteen retrieval cases, i.e. 3 atmospheric scenarios \times 2 observatories \times 3 maximum number of combined transits. We used the nested sampling algorithm Multinest (Feroz et al. 2009) with an evidence tolerance of 0.5 and 750 live points to fit our simulated spectra. We retrieved the following free parameters: planetary radius at 10 bar, atmospheric temperature T_s , water to hydrogen ratio (H_2O/H_2), nitrogen to hydrogen ratio (N_2/H_2) and cloud top pressure (P_{clouds}). For each of the fitted parameters, we used the same uniform priors to avoid biases in the comparison. The retrieved parameters and the priors adopted for the retrievals are listed in Table 5.

3. RESULTS

Figure 1 illustrates the case where four and ten transits of K2-18 b observed with JWST NIRISS and NIRSpec are combined. Figure 2 shows the simulated spectrum of K2-18 b when fifty transits observed with Ariel are combined.

In Figure (3) we show the posterior distributions for two particular cases: JWST 10 observations with NIRISS and NIRSpec and Ariel 50 observations. We find that JWST and Ariel will be able to distinguish among the three scenarios presented in Tsiaras et al. (2019). This is also true in general for the other investigated cases and we report the results of our retrievals in Appendix.

K2-18 b is a small and cold planet orbiting a faint star, therefore it is optimal for JWST sensitivity, but expected to be challenging for Ariel which is optimised for warm and hot planets around bright stars (Edwards et al. 2019b). According to our simulations, with 1 combined NIRISS and NIRSpec observation (2 transits required), JWST should be able to inform on the nature of K2-18 b. Ariel can also reach the same conclusions, but it will require more observations: while 10 combined observations with Ariel start to indicate the atmospheric differences (see Appendix), it is only after 20 combined observations that we distinguish among the three scenarios. 50 combined observations would provide a real insight on the atmospheric composition: this plan would require to observe all transits available during the nominal and extended mission lifetime.

In all the cases analysed here, the water abundance is always well retrieved due to the strong molecular features. The retrieved radius is always very well constrained – less than 2 percent in the worst case of Ariel observing 10 combined transits. Cloud parameters are also retrieved correctly in all the simulations, with very small uncertainties. The temperature, however, is accurately constrained only when we combine more than 5 JWST observations, while all other cases do not converge to the correct solutions and have large uncertainties in the retrieved temperature.

In the case of a secondary atmosphere with water present only as a trace gas, the ratio N_2/H_2 is retrieved correctly. By contrast, the retrievals provide only an upper limit for the N_2 abundance in the 2 other scenarios, i.e. secondary atmosphere with mainly H_2O and primary cloudy atmosphere.

20 combined JWST observations offer very accurate and precise posterior distributions, allowing for an unambiguous characterisation of the atmospheric main gases in K2-18 b, the atmospheric temperature and cloud parameters.

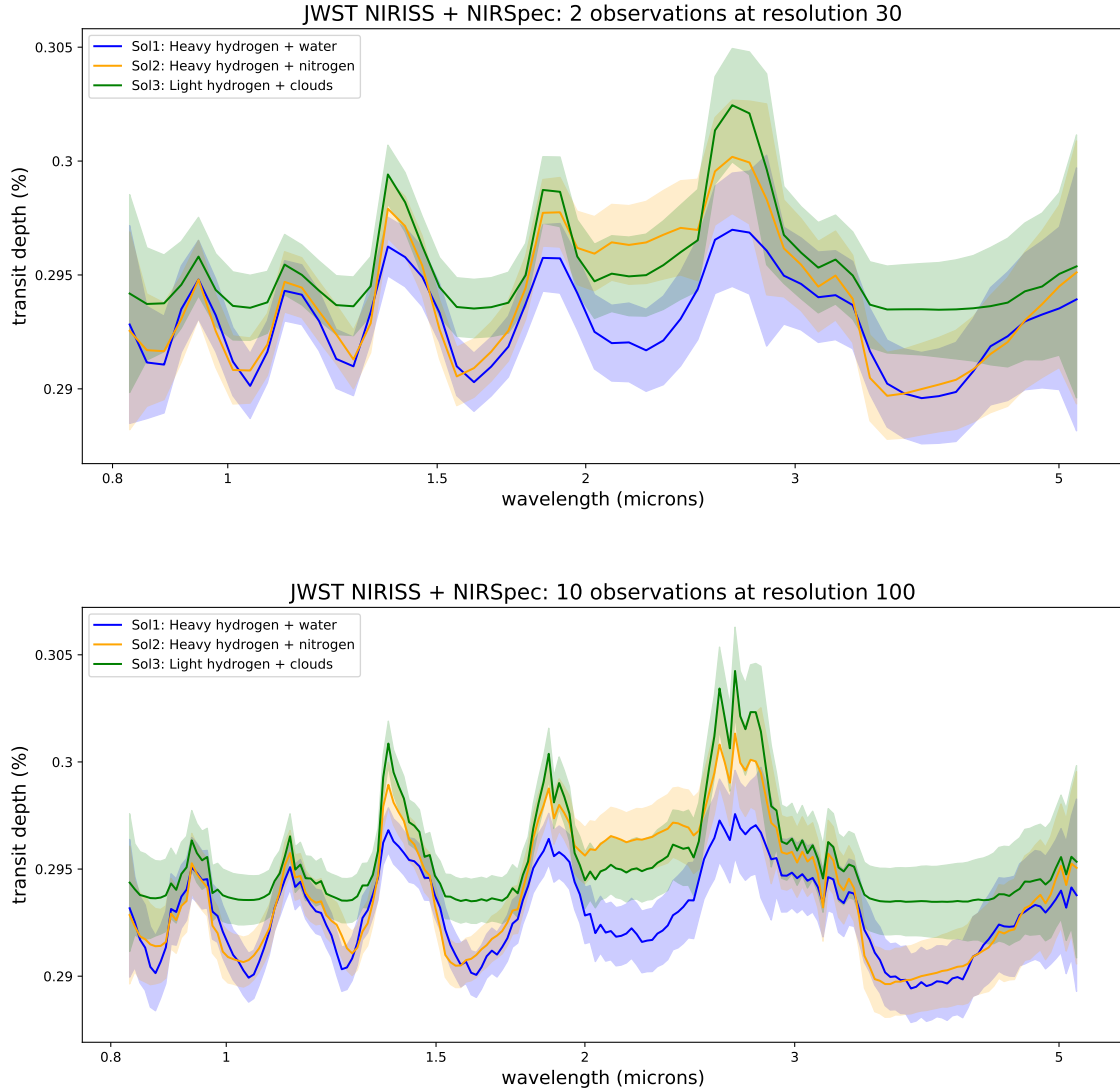


Figure 1. Simulated observed spectra of K2-18b obtained by combining a number of transits recorded with JWST. Top: 2 stacked transits. Bottom: 10 stacked transits.

Finally, we simulated the cases of an atmosphere with a 10 bar, 1 bar and 0.7 bar pressures and we plot the corresponding spectra in Figure 4. This test is important to determine the potential existence of a liquid or a solid surface, and therefore to constrain the nature of the planet. We ran again the retrieval simulations from Tsiaras et al. (2019), which did not assume such surface to exist, using different surface pressures. We found that all 3 surface pressures would still be compatible with the observed WFC3 spectrum and confirm that current observations cannot determine conclusively the nature of the planet. We repeated the experiment for JWST simulated data and show the forward models for the heavy water solution 1 in Figure 5.

Figure 5 shows how for the same planet, the surface pressure influences the observed spectrum. While the observed spectra are different, the changes appear across the entire wavelength range, meaning that they should be very similar to changes in planet radius or cloud pressure. To investigate these degeneracies, we perform two retrievals for the cases with surface pressures of 10 bar and 0.7 bar and attempt to recover information regarding the surface pressure. We set the uniform priors for the retrieved surface pressure from 50 bar to 0.001 bar. The posterior distributions of these two retrievals is presented in Figure 6.

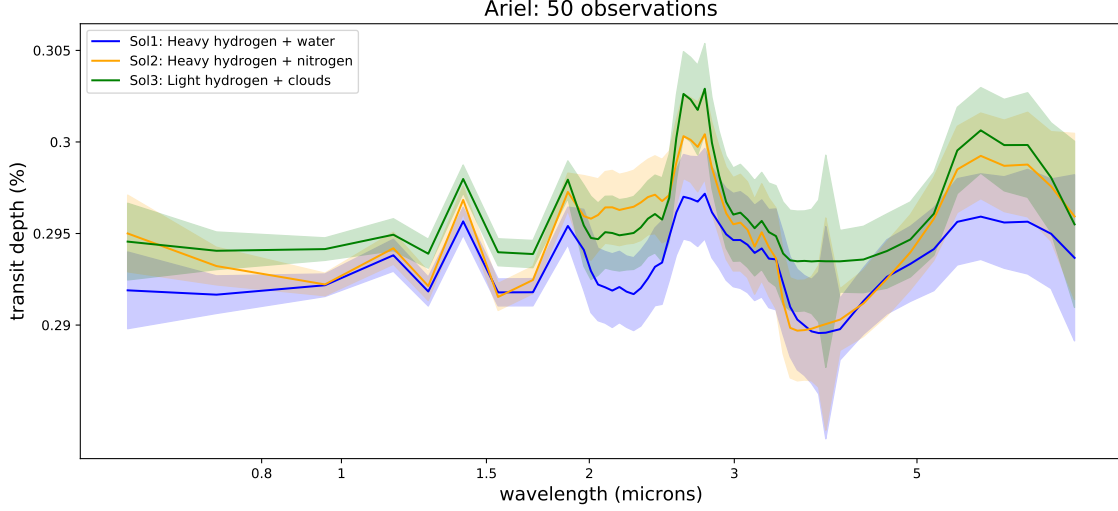


Figure 2. Simulated observed spectra of K2-18b obtained by combining 50 transits recorded with Ariel. If 20 transits are combined, the three scenarios cannot be distinguished.

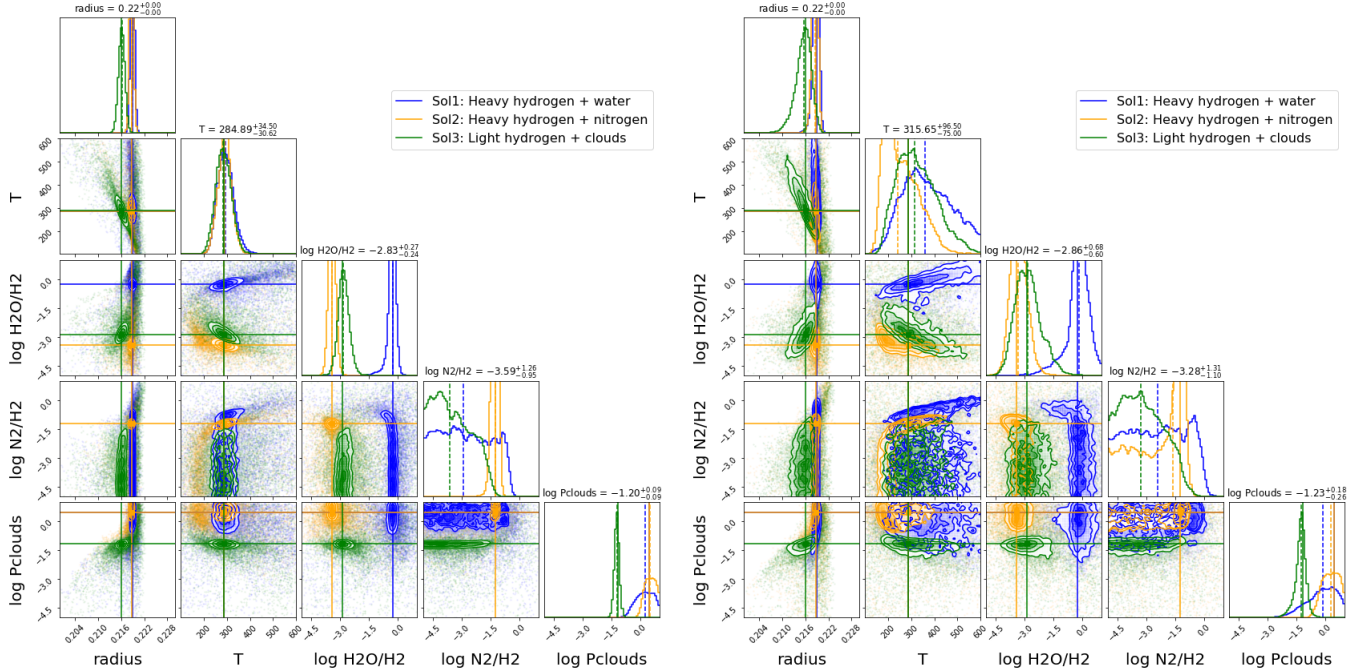


Figure 3. Posteriors related to the three atmospheric scenarios analysed here. Top: 10 combined transits recorded with JWST. Bottom: 50 combined transits recorded with Ariel. In both cases, the three scenarios can be easily distinguished by inspection of the posterior distributions of the parameters.

From the posteriors in Figure 6, one can see that the two retrievals provide very similar posterior distributions. The surface pressure seems to be difficult to constrain directly. The case with surface pressure of 10 bars is unambiguously converging towards a high surface pressure solution, characterised by an upper limit

of around 1bar. The retrieval on the case with surface pressure of 0.7 bar does not provide a definitive answer as it presents two poorly separated modes (see posterior distribution). The first mode is a high pressure with clouds (pressure lower than 1 bar) solution, while the second solution is closer to the true forward model with low surface pressure (peaking at 0.7 bar) and no clouds.

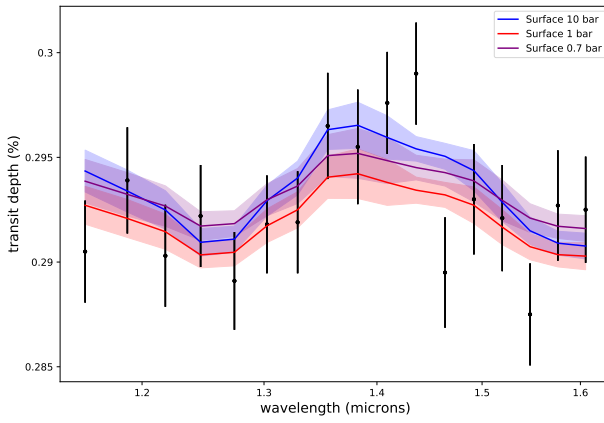


Figure 4. Simulated spectra assuming different surface pressures to interpret the HST-WFC3 observations as published in Tsiaras et al. (2019). Blue plot: 10 bar; red plot: 1 bar; purple plot: 0.7 bar.

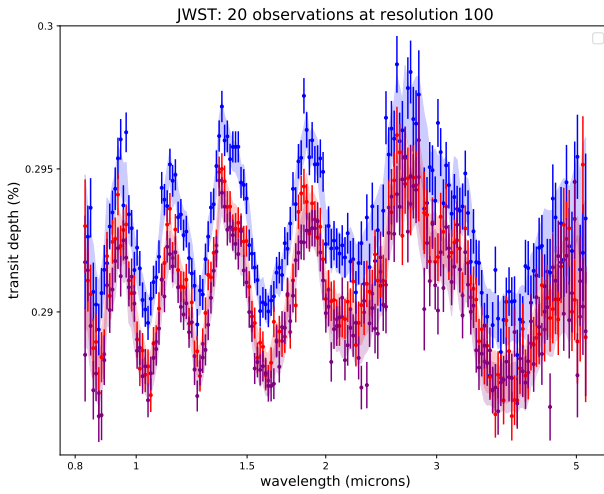


Figure 5. Simulated spectra assuming different surface pressures to interpret JWST simulated observations (20 combined transits). Blue plot: 10 bar; Red plot: 1 bar; Purple plot: 0.7 bar.

This suggests that there are some hints of the lower surface pressure in the simulated spectrum in the Rayleigh scattering part, the Collision Induced Absorption or in the cross sections pressure dependence. However, the characterisation of the surface pressure for cloudy super-Earth planets is likely to be difficult, even in the case of JWST and Ariel.

4. DISCUSSION

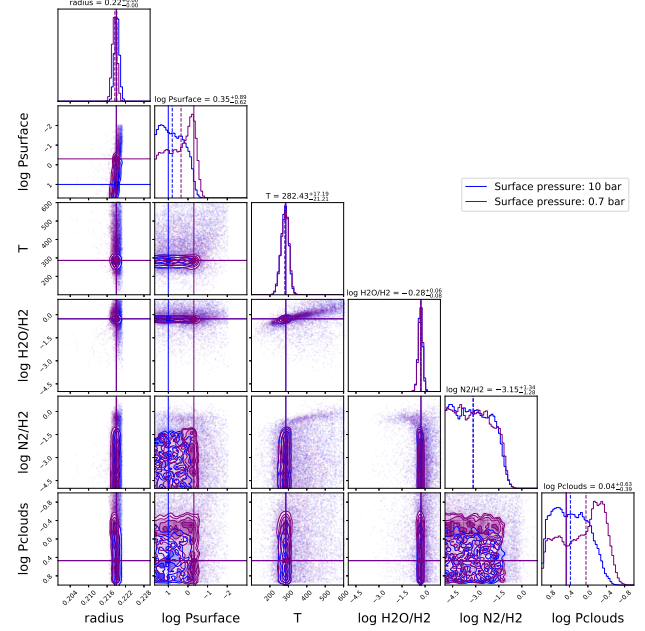


Figure 6. Posteriors for the retrievals where we attempt to recover the surface pressure. Blue: the forward model was using a surface pressure of 10 bar; Purple: the forward model was using a surface pressure of 0.7 bar. The forward models correspond to the ones in Figure 5.

The results presented here suggest that observations with future space infrared observatories will allow to characterise the nature of K2-18b. While current facilities may be limited to disentangle between the three scenarios identified in Tsiaras et al. (2019), as well as to determine whether the planet has a liquid/solid surface or not, complementary observations may provide additional constraints.

- Constraining the Rayleigh/Mie slope:
Additional observations of K2-18b transits in the optical, i.e. $0.3\text{--}0.7\ \mu\text{m}$, could help to constrain the presence of clouds or hazes in this atmosphere. In this spectral region, the data may contain a lot of information concerning the planetary radius and the atmospheric scale height, which could be very informative.
- Reflected light in eclipse observations or phase-curves:
Eclipse observations in the optical could also help to identify and characterise clouds.

In general, clouds increase the planet albedo by reflecting visible light. Mansfield et al. (2019) has shown that cloud reflection could be distinguished from surface reflection by an increased albedo in the case of rocky planets. While this could be an interesting option, they

only investigated surfaces for temperatures higher than 410K. They indeed highlighted the fact that water rich elements (formed at lower temperatures) could have a high albedo, which complicates the interpretation of the results. However, the reflected brightness of a primary atmosphere sub-Neptune or a planet with rocky surface should peak at phase 180° while an ocean world would have a peak brightness around phase 30° (Zugger et al. 2010), providing a direct method to separate these different scenarios. Using TauREx in forward mode, we investigated the thermal emission of K2-18 b and found that the signal (flux ratio of the planet over the star: F_p/F_s) would be lower than 0.01 percent at 50 μm . This means that the emission spectrum of K2-18 b is not observable with JWST. In the case of K2-18 b, reflected light also presents huge challenges. Indeed, the Signal strength for the reflected light case scales as $A_g \left(\frac{R_p}{a} \right)^2$, where A_g is the geometric Albedo and a is the semi-major axis. Since K2-18 b is orbiting far from its host star ($a = 0.14$ AU Cloutier et al. (2017)), the reflected signal is too small to be captured by current and next generation telescopes.

5. CONCLUSIONS

We simulated observations of the low gravity planet K2-18 b as recorded with the next generation of space infrared observatories, i.e. JWST and Ariel. K2-18 b is currently the only planet known in the low gravity regime with a confirmed water vapour detection. The simulations were based on the 3 degenerate solutions identified in Tsiaras et al. (2019) from the Hubble Space Telescope WFC3 observations. By performing a retrieval analysis of these scenarios, we show that the next generation of space telescopes will be able to distinguish among the 3 cases.

The minimum required observations vary from 2 combined observations with NIRISS and NIRSpec for JWST to 20 for Ariel. Increasing the number of observations inevitably leads to better constraint on the atmosphere of K2-18 b. While the chemistry (both main gases and trace elements), temperature and clouds properties of K2-18 b seems to be in reach of the future observatories, our retrieval simulations indicate that the surface pressure may be difficult to directly constrain.

Acknowledgements

This project has received funding from the European Research Council (ERC) under the European Union's

Horizon 2020 research and innovation programme (grant agreement No 758892, ExoAI) and under the European Union's Seventh Framework Programme (FP7/2007-2013)/ ERC grant agreement numbers 617119 (ExoLights). Furthermore, we acknowledge funding by the Science and Technology Funding Council (STFC) grants: ST/K502406/1, ST/P000282/1, ST/P002153/1 and ST/S002634/1.

REFERENCES

Abel, M., Frommhold, L., Li, X., & Hunt, K. L. 2011, *The Journal of Physical Chemistry A*, 115, 6805

—. 2012, *The Journal of chemical physics*, 136, 044319

Al-Refaie et al. 2019, in prep

Barton, E. J., Hill, C., Yurchenko, S. N., et al. 2017, *Journal of Quantitative Spectroscopy and Radiative Transfer*, 187, 453

Benneke, B., Wong, I., Piaulet, C., et al. 2019, arXiv e-prints, arXiv:1909.04642

Changeat, Q., Edwards, B., Waldmann, I., & Tinetti, G. 2019, arXiv e-prints, arXiv:1903.11180

Cloutier, R., Astudillo-Defru, N., Doyon, R., et al. 2017, *A&A*, 608, A35

Cox, A. N. 2015, *Allens astrophysical quantities* (Springer)

Edwards, B., Lagage, P., Gastaud, R., & Al-Refaie, A. 2019a, in prep

Edwards, B., Mugnai, L., Tinetti, G., Pascale, E., & Sarkar, S. 2019b, *AJ*, 157, 242

Feng, Y. K., Robinson, T. D., Fortney, J. J., et al. 2018, *AJ*, 155, 200

Feroz, F., Hobson, M. P., & Bridges, M. 2009, *MNRAS*, 398, 1601

Fletcher, L. N., Gustafsson, M., & Orton, G. S. 2018, *The Astrophysical Journal Supplement Series*, 235, 24

Gordon, I., Rothman, L. S., Wilzewski, J. S., et al. 2016, in *AAS/Division for Planetary Sciences Meeting Abstracts*, Vol. 48, *AAS/Division for Planetary Sciences Meeting Abstracts* #48, 421.13

Mansfield, M., Kite, E. S., Hu, R., et al. 2019, arXiv e-prints, arXiv:1907.13150

Mugnai, L., Edwards, B., & Pascale, E. 2019, in prep

Polyansky, O. L., Kyuberis, A. A., Zobov, N. F., et al. 2018, *Monthly Notices of the Royal Astronomical Society*, 480, 2597

Pontoppidan, K. M., Pickering, T. E., Laidler, V. G., et al. 2016, in *Society of Photo-Optical Instrumentation Engineers (SPIE) Conference Series*, Vol. 9910, *Proc. SPIE*, 991016

Rothman, L. S., & Gordon, I. E. 2014, in *13th International HITRAN Conference*, June 2014, Cambridge, Massachusetts, USA

Tennyson, J., Yurchenko, S. N., Al-Refaie, A. F., et al. 2016, *Journal of Molecular Spectroscopy*, 327, 73, new Visions of Spectroscopic Databases, Volume II. <http://www.sciencedirect.com/science/article/pii/S0022285216300807>

Tsiaras, A., Waldmann, I. P., Tinetti, G., Tennyson, J., & Yurchenko, S. N. 2019, arXiv e-prints, arXiv:1909.05218

Waldmann, I. P., Rocchetto, M., Tinetti, G., et al. 2015a, *ApJ*, 813, 13

Waldmann, I. P., Tinetti, G., Rocchetto, M., et al. 2015b, *ApJ*, 802, 107

Zugger, M. E., Kasting, J. F., Williams, D. M., Kane, T. J., & Philbrick, C. R. 2010, *ApJ*, 723, 1168

APPENDIX
APPENDIX: RETRIEVAL POSTERIORS

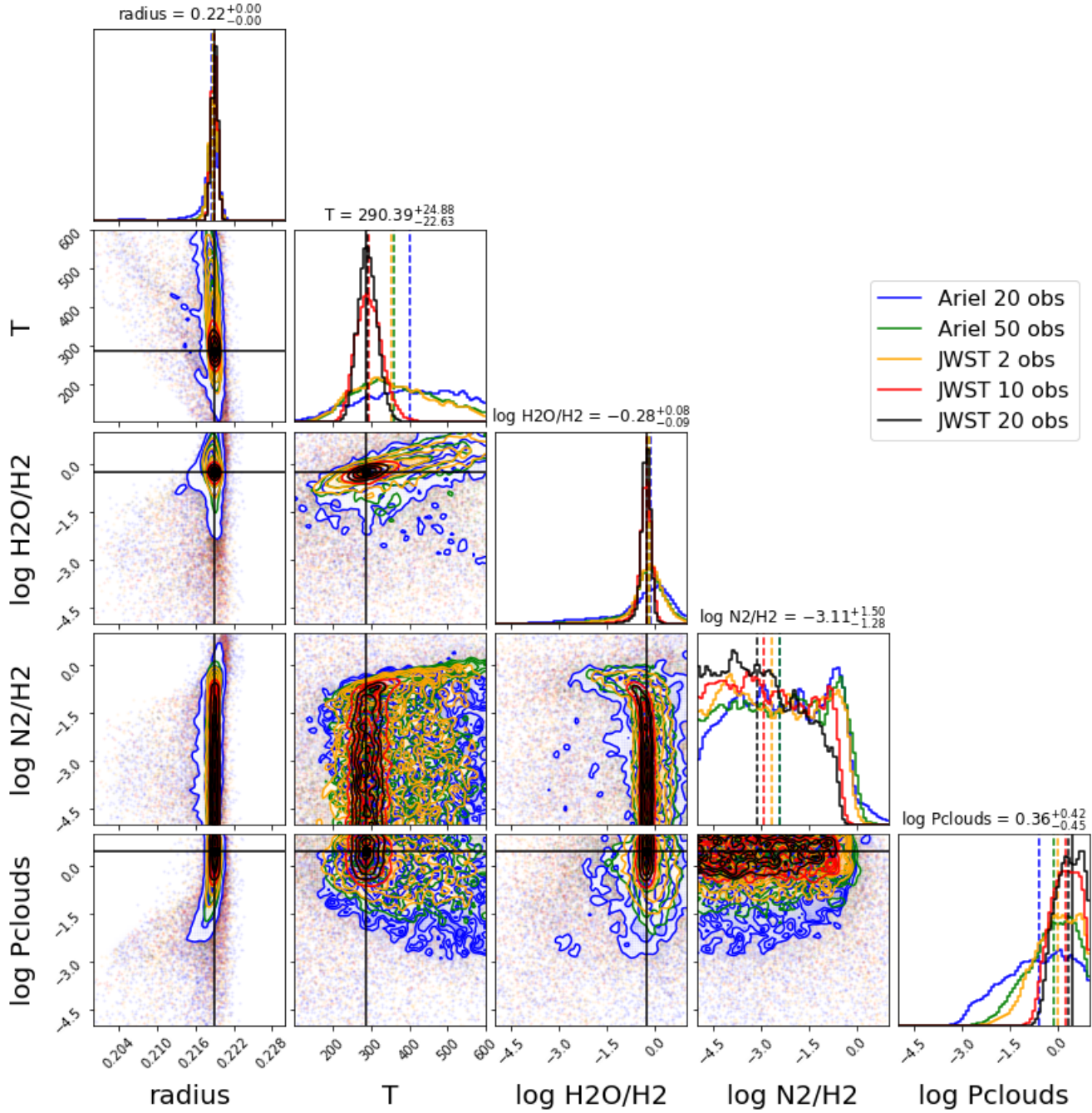


Figure 7. Retrieval posteriors for the atmospheric scenario 1: secondary atmosphere composed of H/He and H₂O.

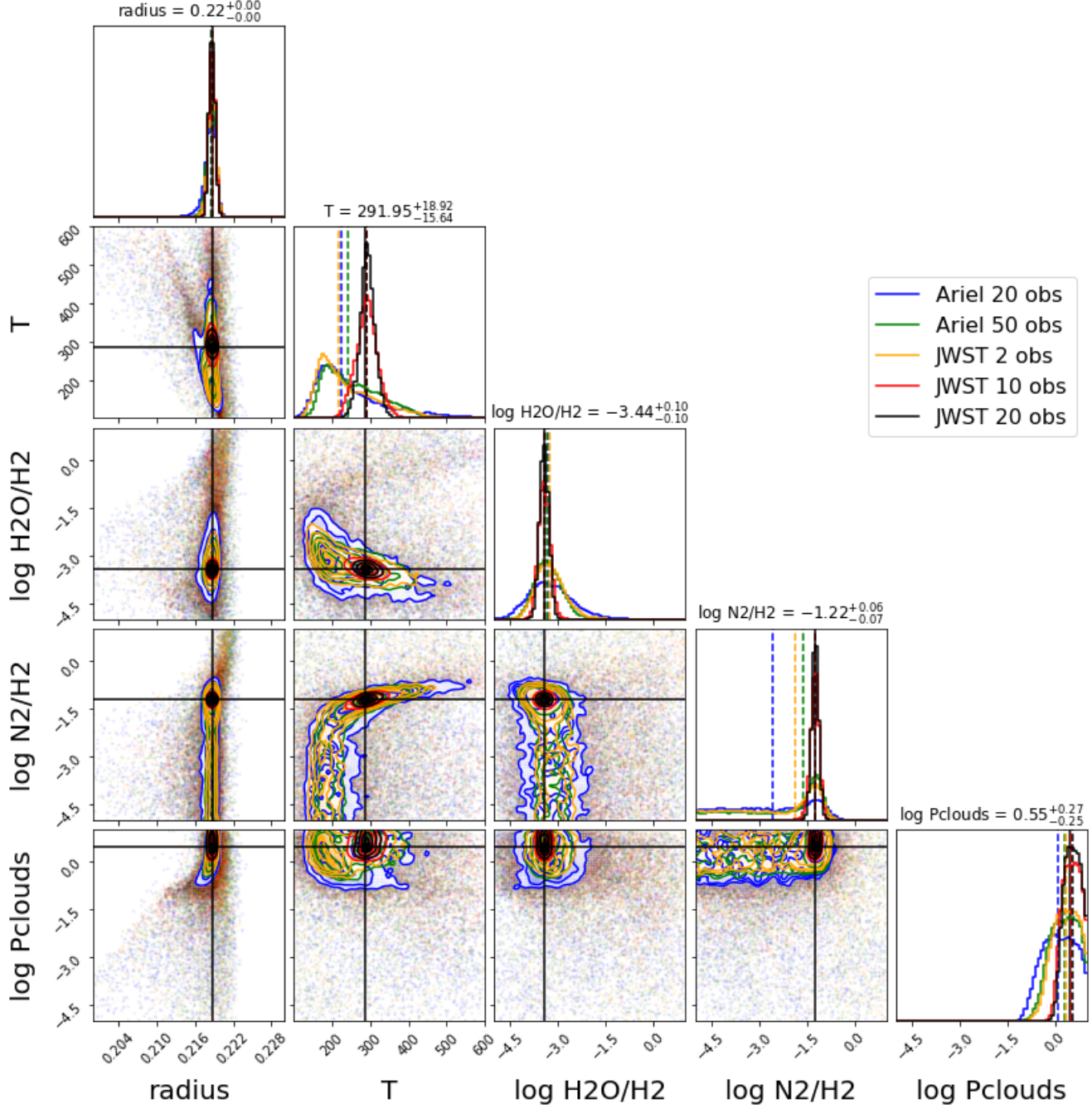


Figure 8. Retrieval posteriors for the atmospheric scenario 2: secondary atmosphere composed of H/He and another undetectable gas, i.e. N₂. Traces of H₂O are also present.

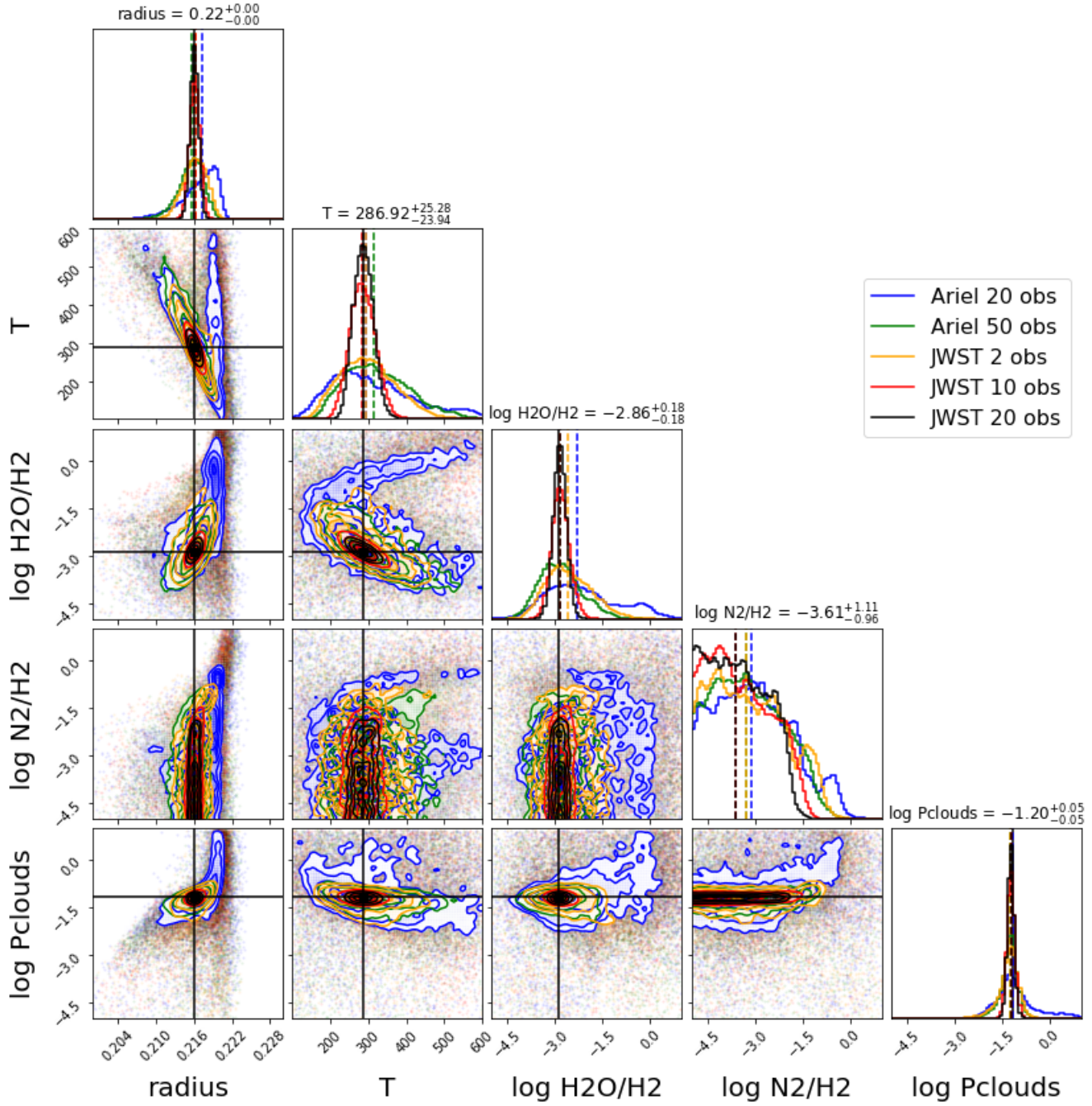


Figure 9. Retrieval posteriors for the atmospheric scenario 3: primary atmosphere composed of H/He and clouds. Traces of H₂O are also present.

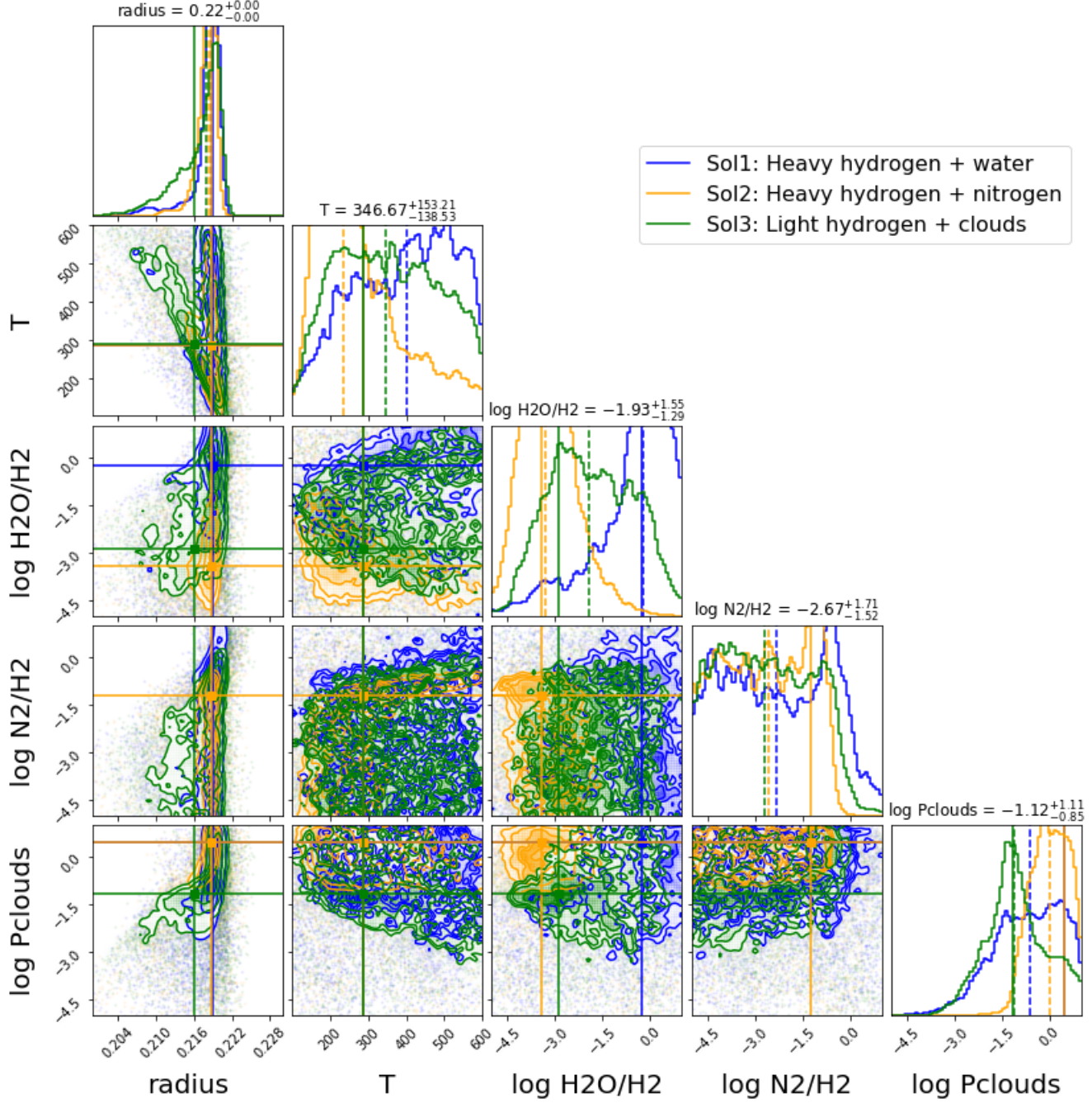


Figure 10. Retrieval posteriors for the 3 scenarios in the case of 10 Ariel transits. The posteriors indicate a departure from a unique solution, however some of the atmospheric parameters are still correlated.